HHS Public Access

Author manuscript

J Cell Biochem. Author manuscript; available in PMC 2022 January 06.

4-hydroxy-2-nonenal attenuates 8-oxoguanine DNA glycosylase 1 activity

Guodong Pan[1,#], **Mandar Deshpande**[1,#], **Haiyan Pang**[1], **Paul M. Stemmer**[3], **Nicholas J Carruthers**[3], **Colin T. Shearn**[4], **Donald S. Backos**[5], **Suresh Selvaraj Palaniyandi**[1,2,*]

[1]Division of Hypertension and Vascular Research, Department of Internal Medicine, Henry Ford Health System, Detroit, MI 48202

[2]Department of Physiology, Wayne State University, Detroit, MI, 48202

[3]Institute of Environmental Health Sciences & Proteomics Facility Core, *Wayne State University,* Detroit, MI, USA, 48201

[4]Department of Pediatrics Division of Pediatric Gastroenterology, Hepatology and Nutrition, School of Medicine, University of Colorado Anschutz Medical Center, Aurora, CO 80045

[5]School of Pharmacy, University of Colorado Anschutz Medical Center, Aurora, CO 80045

Abstract

Elevated cellular oxidative stress and oxidative DNA damage are key contributors to impaired cardiac function in diabetes. During chronic inflammation, reactive oxygen species (ROS)-induced lipid peroxidation results in the formation of reactive aldehydes foremost of which is 4-hydroxy-2-nonenal (4HNE). 4HNE forms covalent adducts with proteins negatively impacting cellular protein function. During conditions of elevated oxidative stress, oxidative DNA damage such as modification by 8-hydroxydeoxyguanosine (8OHdG) is repaired by 8-oxoguanine glycosylase-1 (OGG-1). Based on these facts, we hypothesized that 4HNE forms adducts with OGG-1 and inhibiting its activity, and thus, increasing the levels of 8OHG in the diabetic heart tissues. To test our hypothesis, we evaluated OGG-1 activity, 8OHG and 4HNE in the hearts of leptin receptor

[*]Correspondence: Suresh Selvaraj Palaniyandi, PhD, Division of Hypertension and Vascular Research, Department of Internal Medicine, Education and Research Building, Room 7044, Henry Ford Health System, 2799 West Grand Boulevard, Detroit, MI 48202, Faculty of Physiology, Wayne State University, Tel: 313 916-7055; Fax: 313 916-8759, spalani2@hfhs.org.

Contributions:

Guodong Pan-planned and conducted the animal experiments, performed microscopy and some part of biochemistry and made figures

Mandar Deshpande-planned and conducted the biochemical experiments, figure making and contributed to manuscript writing and editing

Haiyan Pang-immunostaining

Paul M. Stemmer-planned and conducted mass spec studies

Nicholas J Carruthers-analyzed the mass spec data, made figures and contributed to manuscript writing

Colin T. Shearn-planned and conducted molecular modeling studies, made figures and contributed to manuscript writing and editing

Donald S. Backos- planned and conducted molecular modeling studies and made figures

Suresh Selvaraj Palaniyandi-conceived the idea, planned the study, obtained the funding, supervised the experimentation and data analysis, wrote the manuscript and editing.

[#]contributed equally

Data Availability: All the data are within the manuscript and supplementary information.

Duality of Interest: No potential conflicts of interest relevant to this article were reported.

Disclosures: None

deficient *db/db* mice, a type-2 diabetic model. We also treated the recombinant OGG-1 with 4HNE to measure direct adduction. We found decreased OGG-1 activity (P>0.05), increased 8OHG (P>0.05) and increased 4HNE adducts (P>0.05) along with low ALDH2 activity (P>0.05). The increased colocalization of OGG-1 and 4HNE in cardiomyocytes suggest 4HNE adduction on OGG-1. Furthermore, co-localization of 8OHG and OGG-1 with mitochondrial markers TOM 20 and aconitase, respectively indicated significant levels of oxidatively-induced mtDNA damage and implicated a role for mitochondrial OGG-1 function. *In vitro* exposure of recombinant OGG-1 (rOGG-1) with increasing concentrations of 4HNE resulted in a concentration-dependent decrease in OGG-1 activity. Mass spectral analysis of trypsin digests of 4HNE treated rOGG-1 identified 4HNE adducts on C28, C75, C163, H179, H237, C241, K249, H270 and H282. In silico molecular modeling of 4HNE-K249 OGG-1 and 4HNE-H270 OGG-1 mechanistically supported 4HNE-mediated enzymatic inhibition of OGG-1. In conclusion, these data support the hypothesis that inhibition of OGG-1 by direct modification by 4HNE contributes to decreased OGG-1 activity and increased 8OHG-modified DNA that are present in the diabetic heart.

Introduction

The augmented reactive oxygen species (ROS) generation in pathophysiological conditions cause oxidative stress (Droge, 2002). Oxidative stress leads to damage, dysfunction, and disturbances in cellular structures starting from the outer plasma membrane to inner nuclear DNA (Dalton, Shertzer, & Puga, 1999) through a variety of mechanisms. One of the mechanisms is through reactive aldehydes like 4-hydroxy-2-nonenal (4HNE), which are generated upon lipid peroxidation. Lipid peroxides such as 4HNE can form covalent adducts with cellular proteins on cysteine, lysine and histidine residues thereby impairing function (Davies, 2016; Shearn et al., 2013). If cellular antioxidant defenses are inadequate, these modifications can lead to cellular stress and dysfunction. In general, oxidized proteins and RNA are destroyed by cellular machinery. However, oxidative DNA damage is repaired since it is essential for the genomic informational integrity (Bohr, 2002). Oxidative DNA damage can occur on different components of DNA molecules including bases, sugar fragments, abasic/apurinic/apyrimidinic (AP) sites, and single/double-strand breaks (Chatterjee & Walker, 2017). Among the nucleotides, guanine is more susceptible to modification by reactive oxidative intermediates (Delaney, Jarem, Volle, & Yennie, 2012). Oxidative modification of guanine results in the formation of 8-hydroxyguanine (8OHG), 8-hydroxydeoxyguanosine (8OHdG) and 8-oxo-7,8-dihydro-2-deoxyguanosine (8-oxodG). Importantly, these oxidized DNA molecules are established markers of ROS–induced DNA damage (Valavanidis, Vlachogianni, & Fiotakis, 2009).

8-oxoG is one of the most commonly formed oxidative lesions in the cells (Neeley & Essigmann, 2006). It mispairs with A during replication, thus making it a highly mutagenic lesion. (Kino & Sugiyama, 2001). Base excision repair (BER) is one of the primary DNA repair mechanisms (Wallace, 2014). Recently, there are lot of renewed interests developed in DNA repair mechanisms with this topic receiving 2015 Nobel Prize for Chemistry. 8-oxoguanine glycosylases (OGGs) is a group of 8 DNA repair glycosylases. OGG-1 identifies and excises 8OHG and 8-oxoG and imidazole ring-fragmented guanines (FapyG) lesions (Bravard et al., 2006). It is a bifunctional enzyme: In addition to glycosylase activity, it has

lyase activity (Radicella, Dherin, Desmaze, Fox, & Boiteux, 1997). First OGG-1 flips the damaged base out of the DNA double helix and cleaves the N-glycosidic bond of the damaged base (thus called glycosylases), leaving an AP site (McCullough, Dodson, & Lloyd, 1999). Next, OGG-1 executes its lyase activity i.e., cutting the phosphodiester bond of DNA, creating a single-strand break (Boiteux & Guillet, 2004).

An increase in steady-state levels of 8-oxodG in tissues of OGG-1 knockout mice compared with wild-type counterparts implies the importance of OGG-1 activity in keeping the DNA damage in check (Leon et al., 2016). The decrease in OGG-1 activity has been implicated in variety of diseases including cancers, neuro degenerative diseases and metabolic conditions as oxidative stress is prevalent in those diseases (Sampath & Lloyd, 2019). Diabetes-mediated 8-oxodG levels were increased in the kidney tissue of type-1 diabetic rats (Simone, Gorin, Velagapudi, Abboud, & Habib, 2008). Overexpression of OGG-1 prevented fibrosis and ameliorated the type-1 diabetic heart (Wang, Wang, Watson, Jones, & Epstein, 2011). Using the high-fat diet model, Sampath et al showed that increased lipid accumulation in the liver of OGG-1 knockout mice compared to their wild-type counterparts (Sampath et al., 2012). In type-1 and type-2 diabetic models, we found increased 4-hydroxy-2 nonenal (4HNE) protein adducts in the diabetic tissue (Mali et al., 2014; Mali et al., 2016). Previous studies support aberrant post-translational modification of OGG-1 contributes to decreased OGG-1 activity: In type 1 diabetic mice, O-GlcNAcylation of OGG-1 was increased corresponding to decreased OGG-1 activity (Cividini et al., 2016). Therefore, taken altogether we hypothesize that 4HNE decreases OGG-1 activity by forming adducts with OGG-1 on critical sites in diabetic tissue. We tested our hypothesis using recombinant OGG-1 *in vitro* and in the heart tissues of *db/db* mice, a type-2 diabetic model.

Materials and Methods

Experimental animals

Leptin receptor mutant mice, *db/db* (n=12) and their controls, *db/dm* with C57BL/6 background (n=12) were purchased from Jackson Laboratory (Bar Harbor, ME). After 6–9 months, the animals were sacrificed, and heart tissue was isolated. They were appropriately stored for biochemical and histopathological studies. The animal protocols were approved by the Henry Ford Health System Institutional Animal Care and Use Committee. It adheres to the guiding principles of the care and use of experimental animals in accordance with the NIH guidelines. Henry Ford Hospital operates an AAALAC certified animal facility.

Immunostaining of 8OHG

Formalin-fixed, paraffin-embedded cardiac tissue sections were used for immunostaining. After deparaffinization and hydration, the slides were washed in Tris-buffered saline (TBS; 10 mmol/L Tris–HCl, 0.85% NaCl, *p*H 7.5) containing 0.1% bovine serum albumin (BSA). Antigen retrieval was performed using a pressure cooker method at 110 degrees C for 10 minutes. After overnight incubation with mouse 8OHG antibody (Abcam, Cambridge, MA) at a concentration of 1:200 at 4 °C, the slides were washed in TBS. Then we incubated with Goat anti-Mouse IgG Alexa Fluor 488 secondary antibody (Thermo Fisher Scientific, Waltham, MA) for 1 hour in room temperature. After mounting, the stained cardiac sections

were visualized with the help of microscope using Olympus IX81 (Olympus America, Center Valley, PA). The images were captured with a digital camera (DP72) and DPC controller software (Olympus America, Center Valley, PA) set at 488 nm excitation at 40x magnification. We analyzed at least 10 high power images per cardiac section and at least 3 samples per group for quantification.

Immuno co-localization of 4HNE with OGG-1 and 8OHG

Following standard deparaffinization protocol, co-localization of 4HNE with OGG1 and 4HNE with 8OHG was performed by using double immunostaining with 4-HNE-Cys/His/Lys (Millipore Sigma) rabbit antibody (1:200) and OGG-1 mouse monoclonal IgG antibody (1:100) (Santa Cruz Biotechnology, Santacruz, CA). Then, we used secondary antibodies anti-Rabbit IgG Alexa Fluor 568 for red and anti-mouse IgG Alexa Fluor 488 for green (Thermo Fisher Scientific) respectively. Next, for the co-localization of 4HNE with 8OHG, 4-HNE-Cys/His/Lys rabbit antibody (Millipore Sigma) (1: 100) and anti-mouse 8OHG antibody (1: 100) (Abcam) with corresponding secondary antibodies; goat anti-Rabbit IgG Alexa Fluor 488 for green and donkey anti-mouse IgG Alexa Fluor 568 for red were used. Histologic micrograph images were captured using Olympus IX81 (Olympus America, Center Valley, PA). The images were captured with a digital camera (DP72) and DPC controller software (Olympus America, Center Valley, PA) set at 40x magnification. The details of fluorescent single band filters are as follows:

Blue (DAPI) excitation wavelength (Ex): 360–370nm & emission wavelength (Em): 420–460nm; Green (Alexa Flour 488) Ex:460–500nm & Em: 510–560nm; Red (Alexa Flour 488) Ex:533–587nm & Em: 607–682nm. These are same for all florescence imaging done.

OGG-1 expression and purification

Human OGG-1 was expressed and purified from His-tagged constructs as previously described and was the gift of Dr. R. Stephen Lloyd, Oregon Health and Science University (Donley et al., 2015). Purified preparations of OGG1 (>95% pure) were stored at −80°C in 20 mM Tris-HCl (pH 7.0), 100 mM KCl, and 10 mM β-mercaptoethanol, and 50% glycerol.

4HNE treatment and OGG-1 activity assay *in vitro*

The fluorescence-based assay was performed in black, 96-well plates with a final volume of 100 μL per well by following the method described by Donley et al. (Donley et al., 2015). Assay buffer (20 mM Tris-HCl, 100 mM KCl, 0.1% BSA, 0.01% Tween-20, pH 7.5) was added to each well (made up to 100 μL), followed by addition of 1 μL of OGG-1 (pre-diluted in assay buffer + 0.15% Tween) or 200 μg of cell protein, or 4HNE and DMSO in some wells, followed by 1 μl of 2.5 μM double stranded DNA substrate (pre-diluted in assay buffer + 0.15% Tween). The DNA substrate contained a 5′ FAM with an 8-oxoG in at nucleotide 6, annealed to a complementary strand containing a 3′ BHQ-1 (custom synthesized by Integrated DNA technologies (IDT) Coralville, Iowa). The 4HNE (100 μM) treated wells were first incubated with OGG-1 and then with 4HNE for 1 hr at room temperature, before the addition of DNA substrate. The final concentration of each component in the reaction was 100 μM 4HNE, 50 nM enzyme, and 25 nM substrate. After the addition of DNA substrate, plates were incubated at room temperature for 10 minutes,

and then FAM fluorescence was measured in a Synergy H1 plate reader (Ex: 494; Em: 520) for 1 hour, with readings taken at every 20 minutes interval. Total OGG-1 activity per well was calculated by background-subtraction (buffer and buffer + substrate DNA) of fluorescence values from each well.

We also measured OGG-1 activity in the cardiac tissue homogenate from control and diabetic mice using the same assay.

Western immunoblotting

The western blot was performed as described earlier (Mali et al., 2016; Pan, Deshpande, Thandavarayan, & Palaniyandi, 2016). In brief, protein samples from heart tissue homogenate were separated on SDS-polyacrylamide gels by electrophoresis. The proteins were then transferred to immobilon-P membranes (Millipore, Billerica, MA). 4HNE-protein adduct levels were determined using antibodies of anti-4HNE-Cys/His/Lys rabbit antibody (Millipore Sigma, Burlington, MA) (at a concentration of 1:1000) and porin mouse monoclonal antibody at a concentration of 1:2000 (Abcam) was used as a housekeeping marker, for comparison. The bound primary antibodies were added to horseradish peroxidase (HRP)-coupled respective secondary antibodies, and then visualized by chemiluminescence detection reagents.

Immuno co-localization of 8OHG and OGG-1 with mitochondrial markers

Cardiac paraffin sections were deparaffinized as mentioned above. Then, the co-immuno localization of 8OHG and OGG-1 with mitochondrial markers TOM20 and aconitase respectively was performed. First, the double immunostaining with primary antibodies of 8OHG; anti-mouse 8OHG antibody (1:100) (Abcam) and Tom 20; anti-rabbit TOM 20 antibody (SantaCruz) (1:100) were used along with respective secondary antibodies, anti-mouse IgG Alexa Fluor 488 for green and anti-Rabbit IgG Alexa Fluor 568 for red (Thermo Fischer). Similarly, for the double staining of OGG-1 and aconitase, the primary antibodies: anti-rabbit OGG-1 antibody (Novus Biologicals, LLC Centennial CO) and anti-mouse aconitase antibody (Abcam) along with respective secondary antibodies, anti-rabbit IgG Alexa Fluor 488 for green and anti-mouse IgG Alexa Fluor 568 for red (Thermo Fischer) were used. See above for microscopic and imaging details.

Mass spectrometry analysis of recombinant OGG-1 incubated with 4HNE

Recombinant OGG-1 protein was treated with 0, 10 or 100 μM 4HNE and 10 ug aliquots of each were buffered with 50 mM ammonium bicarbonate (AMBIC). 4HNE adducts were stabilized by reaction with 5 mM $NaBH_4$ in equimolar NaOH. Following the $NaBH_4$ reaction cysteines were reduced with 5 mM dithiothreitol (DTT) then alkylated with 15 mM iodoacetamide (IAA). Excess IAA was quenched with a second addition of 5 mM DTT. Samples were digested at 37 C overnight using sequencing-grade trypsin (Promega, Madison, WI). Following digestion all samples were speedvac to dryness and solubilized in 0.1% FA in preparation for LC-MS/MS. All analyses were made using an Acclaim PepMap RSLC, 75 um × 25 cm column with LC-MS/MS performed on a Thermo Fusion orbitrap mass spectrometer. 35-minute LC gradients were used, MS1 scans were collected at 120K

resolution and the most abundant species were selected for MS2 analysis by CID in the ion trap.

Protein and modified site identification

Mass spectrometer raw files were searched using PEAKS Studio 8.5 build 20180507 against the Uniprot/TrEMBL human database (20 145 entries entries) using 10 ppm precursor mass tolerance and 0.6 Da product mass tolerance against a human database. PEAKS PTM was used to identify modified peptides using a panel of 313 variable modifications including 4HNE on C, H, and K (156.1150 Da addition). Carbamidomethylated C (57.0215 Da addition) was also set as a variable modification. PTM localization confidence was determined by PEAKS PTM. Quantification was done using chromatographic peak area for the precursor. Data analysis was done in R v3.4.3 and excel.

Molecular Modeling

All simulations were performed using Discovery Studio version 2.5.5 (Accelrys Inc., San Diego, CA). The crystallographic coordinates of the 3.1 Å human 8-oxoguanine glycosylase distally cross-linked to guanine crystal structure (Protein Data Bank entry 3ih7 (Crenshaw et al., 2012)) were obtained from the Protein Data Bank (http://wwww.rcsb.org). The 4HNE modification of the K249 and H270 residues of OGG-1 (Crenshaw et al., 2012; van der Kemp, Charbonnier, Audebert, & Boiteux, 2004) was completed as follows: The resulting structure was then subjected to energy minimization utilizing the conjugate gradient minimization protocol (10,000 iterations) with a CHARM forcefield and the Generalized Born implicit solvent model with simple switching (Feig et al., 2004). Schiff base adducts of 4HNE were built onto K249 and H270 as identified by MS/MS analysis and both the native and adducted models subjected to a further round of minimization as described above.

Statistical analysis

Data are presented as mean ± standard error of the mean (SEM). The student’s t test was applied to compare the two groups in the studies.

Results

Diabetes increases 8OHG levels in the mitochondria of the heart tissue

8OHG levels were increased in the *db/db* mouse heart compared to *db/dm* mouse hearts (Figures 1A &1D, 1C&1G, 1E & 1H and 1I). Moreover, 8OHG was colocalized with the mitochondria as shown by TOM20, a mitochondrial protein (Figures 1B & 1F, 1C&1G, 1D & 1H)

Diabetes decreases OGG-1 activity in heart tissue

OGG-1 activity was reduced in the *db/db* diabetic hearts compared that of *db/dm* hearts (Fig 2).

Significant amount of OGG-1 was colocalized with mitochondrial marker protein aconitase which is suggesting mtOGG-1.

4HNE adducts are increased along with decrease in ALDH2 activity in diabetic heart

Increased 4HNE adducts (Fig. 3A) and decreased ALDH2 activity (Fig. 3B) in *db/db* hearts were found relative to *db/dm* control hearts.

4HNE adducts are increased in OGG-1 in diabetic heart tissues.

Increases in 4HNE protein adducts on OGG-1 protein were found in the *db/db* hearts compared to the *db/dm hearts* (Fig. 4A–4I).

Exogenous 4HNE attenuates recombinant OGG-1 activity

Recombinant OGG-1 activity was reduced with 4HNE (1, 10 and 100 μM) in a dose-dependent manner (Fig. 5A). Recombinant OGG-1 activity was lower in 20, 40 and 60 minutes with 100 μM 4HNE compared to vehicle treatment (Fig. 5B).

4HNE adduct formation in OGG1 by mass spectroscopy

Treatment of recombinant OGG1 with 4HNE resulted in the formation of HNE adducts (Fig. 6A). No 4HNE adducts were detected in untreated samples indicating our analysis is specific. Peptide abundances for HNE modified peptides in treated samples were determined using label-free quantification (Fig. 6B).

Identification of 4HNE adducted residues in OGG-1

We identified C28, C75, C163, H179, H237, C241, K249, H270 and H282 in the OGG-1 protein structure (Fig. 7).

Molecular structural analysis of 4HNE adduction on OGG-1

The relative location of each adducted amino acid identified and its special relation to the DNA binding sites was first examined using a known crystal structure of OGG-1 (Figure S3) (Crenshaw et al., 2012). From the special comparison as well as that fact that both K249 and H270 have previously been demonstrated to be important in OGG-1 activity (Radom, Banerjee, & Verdine, 2007; van der Kemp et al., 2004), computational-based minimization simulations were performed focusing on the aforementioned residues using the crystal structure of OGG-1 bound to 8-oxo-7,8-dihydroguanine (8-oxoG) modified DNA (3ih7 (Crenshaw et al., 2012)). Using *in silico* molecular modeling, 4HNE was adducted to K249 and H270 on human OGG-1. From the prediction of amino acid pKa values, H270 is protonated resulting in increased susceptibility to adduction. These results demonstrate that the charged nitrogen is the more likely target and addition of the 4HNE would abrogate the charge on the Histidine residue, impacting the interaction with the DNA backbone (Figure 8A and 8B). Examining adduction of K249, the addition of 4HNE alters both the positioning of the base of the DNA in the catalytic pocket, and abrogates the strong pi-cation interactions that K249 has with the base itself (Figure 8A, 8C-Red arrow). This would directly impact enzymatic activity correlating with data demonstrating a 4HNE concentration-dependent inhibition of OGG-1 activity. Surprisingly, adduction of K249 did not impact the formation of H-bonds between K249 and Cys253 (Figure S4). This was also not impacted by the theoretical simultaneous double adduction of both K249 and H270

(Figure 8D). This would directly impact enzymatic activity correlating with data demonstrating a 4HNE concentration-dependent inhibition of OGG-1 activity.

Discussion

In this study, we found increased 4HNE adduction on OGG-1 and reduction in its activity in type-2 diabetic heart tissue along with enhanced oxidatively-induced mitochondrial DNA damage i.e. increased 8OHG levels. Moreover, exogenous 4HNE attenuates OGG-1 activity by forming adducts on critical amino acids in the OGG-1.

Diabetes and its complications are major healthcare issue in the globe and ~65% of diabetic people die of heart diseases. Since oxidative stress has been identified as an important contributing factor for the diabetic heart diseases, we plan to focus on 4HNE-mediated molecular mechanism in OGG-1 impairment and resultant 8OHG levels.

An increase in DNA oxidative damage in the liver of streptozotocin (STZ)-induced type-1 diabetic rat was reported earlier (Andican & Burcak, 2005). In another report using the same STZ model, it was shown that OGG-1 level was reduced in the kidney cortex (Simone et al., 2008). However, our study is first to report increased oxidative mitochondrial DNA damage in the heart of *db/db* mice, a model of type-2 diabetic mice. In a previous study, by feeding a high-fat diet to OGG-1 knockout mice, Sampath et al found that the develop glucose intolerance, lipid accumulation in the liver and obesity compared to their wild-type counterparts (Sampath et al., 2012). This study implicates the role of OGG-1 in the development of type-2 diabetes. A genetic polymorphism on OGG-1 i.e. S326C OGG-1 is associated with type 2 diabetes in humans (Thameem et al., 2010). Our objective was to establish the association between mtOGG-1 activity and 8OHG levels in the type-2 diabetic heart.

We found that the 8OHG, an oxidized DNA molecule and TOM20, a mitochondrial marker protein, colocalized in diabetic heart tissue implicating it is mtDNA damage. This finding is in accordance with another report in which they found a significant increase in 8oxodG in the mitochondrial fractions of the kidney cortex of STZ-mediated type-1 diabetic rats, but not the nuclear fractions (Simone et al., 2008). We also found that OGG-1 was co-localized with aconitase, another mitochondrial marker, again implicating we have mtOGG-1. Although we found OGG-1 activity was significantly decreased in diabetic hearts compared to control hearts, we did not observe any decrease in mtOGG-1 levels in diabetic hearts compared to non-diabetic control hearts. This made us look for a novel mechanism for OGG-1 impairment in type 2 diabetic heart.

The attack by free radicals on biological membranes is called lipid peroxidation which produces reactive aldehydes like 4HNE. 4HNE forms adduct with macromolecules primarily with proteins and thereby affect their function. In this study, we found that an increase in 4HNE protein adducts in diabetic heart tissue by both Western blot and immunostaining. Additionally, we also found a decrease in the activity of aldehyde dehydrogenase (ALDH) 2, a mitochondrial enzyme that detoxifies 4HNE. This may be another reason why these 4HNE adduct levels are increased in the diabetic heart. We also found this 4HNE adducts are

colocalized with OGG-1 (Fig 3) and 8OHG (supplementary figure 2), which implicating the 4HNE adduct formation in OGG-1 which perhaps increased 8OHG due to reduced OGG-1 activity due to 4HNE adduction on critical sites. In an earlier report, it has been shown that in the vulnerable regions of the brains of patients with Alzheimer's disease, OGG-1 activity is reduced due to 4HNE adduction (Montine et al., 2002). In this study, it was both mitochondrial and nuclear OGG-1. However, it is unknown at which sites 4HNE forms adducts with OGG-1. To determine this, we performed few *in vitro* studies with recombinant OGG-1 activity. Treatment with 4HNE (1, 10 and 100 μM) attenuated OGG-1 activity in a dose-dependent manner *in vitro*. Montine et al. have incubated the control brain lysates that had highest OGG-1 activity with 5 μM 4HNE for 1 hour and found that OGG-1 activity was decreased ~50% implicating 4HNE can form adducts with OGG-1 readily and inhibits its activity significantly.

As we found 10 and 100 μM decreased OGG-1 activity significantly, we then incubated OGG-1 with 10 to 100 μM 4HNE and performed mass spectroscopy. As expected, we found 4HNE modifications in specific peptides with 10 and 100 μM 4HNE compared to control. We identified four such peptides. Next, we identified specific amino acid residues in those peptides which had 4HNE adductions. They included the amino acids C28, C75, C163, H179, H237, C241, K249, H270 and H282. Among these residues, K249 is known as a catalytic site for OGG-1. It is important to understand the biochemistry of these sites in terms of how base excision repair by OGG-1 is executed by recognizing and discriminating against the DNA lesions. There was a previous study published on mutations with some critical residues of OGG-1 and their importance on accessing and repairing the oxidized DNA such as 8-oxodG (Radom et al., 2007). In that study, they have also mutated H270 and K249. The inference from these mutations is: 1) H270A mutation diminishes the affinity of hOGG-1 for tetrahydrofuranyl-containing DNA by less than 2-fold. 2) K249Q, a catalytic nucleophile did not interact with C253. This interaction is essential for the specific recognition of oxoG (Radom et al., 2007). Based on this biochemical structural study, we presume that the decrease in OGG-1 activity in diabetic heart tissue was due to 4HNE adductions on these critical sites.

Next, we performed *in silico* analysis to build molecular modeling simulations of the 4HNE adductions on those amino acids of OGG-1 along with its substrate to understand how 4HNE adductions can affect the function of OGG-1 at the biochemical level. Molecular modelling revealed two possible mechanisms of 4HNE-mediated attenuation of OGG-1 activity. First, modification of H270 would impact the ability of OGG-1 to associate with the DNA backbone. Second, adduction of K249 would impact OGG-1/8-oxoG substrate interactions and therefore catalysis.

In summary, in this report we have for the first time found mtOGG-1 activity is reduced and which increased 8OHG in the mitochondria of cardiac tissue procured from diabetic db/db mice. Concurrently, from *in vitro* studies using recombinant protein, we have identified 4HNE adduction sites on the OGG-1 and determined plausible mechanisms of 4HNE-mediate OGG-1 inhibition. Thus, in the future, determining whether protecting those specific sites from 4HNE adduction can decrease mtOGG-1 inactivation. Since the mitochondrial ALDH2 detoxifies 4HNE, activation of ALDH2 may be an effective strategy

to improve mtOGG-1 activity in the diabetic heart. Finally, in conclusion, we propose that 4HNE attenuates mtOOG1 activity by forming adducts with critical amino acids, which can be decreased by enhancing 4HNE detoxification.

Supplementary Material

Refer to Web version on PubMed Central for supplementary material.

Acknowledgments:

We thank Oskar Linde and Stephan Lloyd from Oregon Institute of Occupational Health Sciences, Oregon Health & Science University Portland, Oregon for the gift of recombinant hOGG-1 protein.

Funding Source: This work was partially supported by National Heart, Lung, and Blood Institute 1R01HL139877–01A1 (SSP), National Heart, Lung, and Blood Institute 1 R56 HL131891–01A1 (SSP) and an internal grant from Henry Ford Health System: A10249 (SSP). National Institute of Alcohol Abuse and Alcoholism R37AA009300–22 (CTS). The Wayne State University Proteomics Core Facility is supported by NIH grants P30 ES020957, P30 CA 022453 and S10 OD010700.

References

Andican G, & Burcak G. (2005). Oxidative damage to nuclear DNA in streptozotocin-diabetic rat liver. Clin Exp Pharmacol Physiol, 32(8), 663–666. Retrieved from https://www.ncbi.nlm.nih.gov/pubmed/16120194. doi:10.1111/j.0305-1870.2005.04247.x [PubMed: 16120194]

Bohr VA (2002). Repair of oxidative DNA damage in nuclear and mitochondrial DNA, and some changes with aging in mammalian cells. Free Radic Biol Med, 32(9), 804–812. Retrieved from https://www.ncbi.nlm.nih.gov/pubmed/11978482. [PubMed: 11978482]

Boiteux S, & Guillet M. (2004). Abasic sites in DNA: repair and biological consequences in Saccharomyces cerevisiae. DNA Repair (Amst), 3(1), 1–12. Retrieved from https://www.ncbi.nlm.nih.gov/pubmed/14697754. [PubMed: 14697754]

Bravard A, Vacher M, Gouget B, Coutant A, de Boisferon FH, Marsin S, . . . Radicella JP (2006). Redox regulation of human OGG1 activity in response to cellular oxidative stress. Mol Cell Biol, 26(20), 7430–7436. Retrieved from https://www.ncbi.nlm.nih.gov/pubmed/16923968. doi:10.1128/MCB.00624-06 [PubMed: 16923968]

Chatterjee N, & Walker GC (2017). Mechanisms of DNA damage, repair, and mutagenesis. Environ Mol Mutagen, 58(5), 235–263. Retrieved from https://www.ncbi.nlm.nih.gov/pubmed/28485537. doi:10.1002/em.22087 [PubMed: 28485537]

Cividini F, Scott BT, Dai A, Han W, Suarez J, Diaz-Juarez J, . . . Dillmann WH (2016). O-GlcNAcylation of 8-Oxoguanine DNA Glycosylase (Ogg1) Impairs Oxidative Mitochondrial DNA Lesion Repair in Diabetic Hearts. J Biol Chem, 291(51), 26515–26528. Retrieved from https://www.ncbi.nlm.nih.gov/pubmed/27816939. doi:10.1074/jbc.M116.754481 [PubMed: 27816939]

Crenshaw CM, Nam K, Oo K, Kutchukian PS, Bowman BR, Karplus M, & Verdine GL (2012). Enforced presentation of an extrahelical guanine to the lesion recognition pocket of human 8-oxoguanine glycosylase, hOGG1. J Biol Chem, 287(30), 24916–24928. Retrieved from https://www.ncbi.nlm.nih.gov/pubmed/22511791. doi:10.1074/jbc.M111.316497 [PubMed: 22511791]

Dalton TP, Shertzer HG, & Puga A. (1999). Regulation of gene expression by reactive oxygen. Annu Rev Pharmacol Toxicol, 39, 67–101. Retrieved from https://www.ncbi.nlm.nih.gov/pubmed/10331077. doi:10.1146/annurev.pharmtox.39.1.67 [PubMed: 10331077]

Davies MJ (2016). Protein oxidation and peroxidation. Biochem J, 473(7), 805–825. Retrieved from https://www.ncbi.nlm.nih.gov/pubmed/27026395. doi:10.1042/BJ20151227 [PubMed: 27026395]

Delaney S, Jarem DA, Volle CB, & Yennie CJ (2012). Chemical and biological consequences of oxidatively damaged guanine in DNA. Free Radic Res, 46(4), 420–441. Retrieved from https://www.ncbi.nlm.nih.gov/pubmed/22239655. doi:10.3109/10715762.2011.653968 [PubMed: 22239655]

Donley N, Jaruga P, Coskun E, Dizdaroglu M, McCullough AK, & Lloyd RS (2015). Small Molecule Inhibitors of 8-Oxoguanine DNA Glycosylase-1 (OGG1). ACS Chem Biol, 10(10), 2334–2343. Retrieved from https://www.ncbi.nlm.nih.gov/pubmed/26218629. doi:10.1021/acschembio.5b00452 [PubMed: 26218629]

Droge W. (2002). Free radicals in the physiological control of cell function. Physiol Rev, 82(1), 47–95. Retrieved from https://www.ncbi.nlm.nih.gov/pubmed/11773609. doi:10.1152/physrev.00018.2001 [PubMed: 11773609]

Feig M, Onufriev A, Lee MS, Im W, Case DA, & Brooks CL 3rd. (2004). Performance comparison of generalized born and Poisson methods in the calculation of electrostatic solvation energies for protein structures. Journal of computational chemistry, 25(2), 265–284. Retrieved from http://www.ncbi.nlm.nih.gov/pubmed/14648625. doi:10.1002/jcc.10378 [PubMed: 14648625]

Kino K, & Sugiyama H. (2001). Possible cause of G-C-->C-G transversion mutation by guanine oxidation product, imidazolone. Chem Biol, 8(4), 369–378. Retrieved from https://www.ncbi.nlm.nih.gov/pubmed/11325592. [PubMed: 11325592]

Leon J, Sakumi K, Castillo E, Sheng Z, Oka S, & Nakabeppu Y. (2016). 8-Oxoguanine accumulation in mitochondrial DNA causes mitochondrial dysfunction and impairs neuritogenesis in cultured adult mouse cortical neurons under oxidative conditions. Sci Rep, 6, 22086. Retrieved from https://www.ncbi.nlm.nih.gov/pubmed/26912170. doi:10.1038/srep22086 [PubMed: 26912170]

Mali VR, Ning R, Chen J, Yang XP, Xu J, & Palaniyandi SS (2014). Impairment of aldehyde dehydrogenase-2 by 4-hydroxy-2-nonenal adduct formation and cardiomyocyte hypertrophy in mice fed a high-fat diet and injected with low-dose streptozotocin. Exp Biol Med (Maywood), 239(5), 610–618. Retrieved from https://www.ncbi.nlm.nih.gov/pubmed/24651616. doi:10.1177/1535370213520109 [PubMed: 24651616]

Mali VR, Pan G, Deshpande M, Thandavarayan RA, Xu J, Yang XP, & Palaniyandi SS (2016). Cardiac Mitochondrial Respiratory Dysfunction and Tissue Damage in Chronic Hyperglycemia Correlate with Reduced Aldehyde Dehydrogenase-2 Activity. PLoS One, 11(10), e0163158. Retrieved from https://www.ncbi.nlm.nih.gov/pubmed/27736868. doi:10.1371/journal.pone.0163158

McCullough AK, Dodson ML, & Lloyd RS (1999). Initiation of base excision repair: glycosylase mechanisms and structures. Annu Rev Biochem, 68, 255–285. Retrieved from https://www.ncbi.nlm.nih.gov/pubmed/10872450. doi:10.1146/annurev.biochem.68.1.255 [PubMed: 10872450]

Montine TJ, Neely MD, Quinn JF, Beal MF, Markesbery WR, Roberts LJ, & Morrow JD (2002). Lipid peroxidation in aging brain and Alzheimer's disease. Free Radic Biol Med, 33(5), 620–626. Retrieved from https://www.ncbi.nlm.nih.gov/pubmed/12208348. doi:10.1016/s0891-5849(02)00807-9 [PubMed: 12208348]

Neeley WL, & Essigmann JM (2006). Mechanisms of formation, genotoxicity, and mutation of guanine oxidation products. Chem Res Toxicol, 19(4), 491–505. Retrieved from https://www.ncbi.nlm.nih.gov/pubmed/16608160. doi:10.1021/tx0600043 [PubMed: 16608160]

Pan G, Deshpande M, Thandavarayan RA, & Palaniyandi SS (2016). ALDH2 Inhibition Potentiates High Glucose Stress-Induced Injury in Cultured Cardiomyocytes. J Diabetes Res, 2016, 1390861. Retrieved from https://www.ncbi.nlm.nih.gov/pubmed/27882330. doi:10.1155/2016/1390861

Radicella JP, Dherin C, Desmaze C, Fox MS, & Boiteux S. (1997). Cloning and characterization of hOGG1, a human homolog of the OGG1 gene of Saccharomyces cerevisiae. Proc Natl Acad Sci U S A, 94(15), 8010–8015. Retrieved from https://www.ncbi.nlm.nih.gov/pubmed/9223305. [PubMed: 9223305]

Radom CT, Banerjee A, & Verdine GL (2007). Structural characterization of human 8-oxoguanine DNA glycosylase variants bearing active site mutations. J Biol Chem, 282(12), 9182–9194. Retrieved from https://www.ncbi.nlm.nih.gov/pubmed/17114185. doi:10.1074/jbc.M608989200 [PubMed: 17114185]

Sampath H, & Lloyd RS (2019). Roles of OGG1 in transcriptional regulation and maintenance of metabolic homeostasis. DNA Repair (Amst), 81, 102667. Retrieved from https://www.ncbi.nlm.nih.gov/pubmed/31311771. doi:10.1016/j.dnarep.2019.102667

Sampath H, Vartanian V, Rollins MR, Sakumi K, Nakabeppu Y, & Lloyd RS (2012). 8-Oxoguanine DNA glycosylase (OGG1) deficiency increases susceptibility to obesity and metabolic

dysfunction. PLoS One, 7(12), e51697. Retrieved from https://www.ncbi.nlm.nih.gov/pubmed/23284747. doi:10.1371/journal.pone.0051697

Shearn CT, Smathers RL, Backos DS, Reigan P, Orlicky DJ, & Petersen DR (2013). Increased carbonylation of the lipid phosphatase PTEN contributes to Akt2 activation in a murine model of early alcohol-induced steatosis. Free Radic Biol Med, 65, 680–692. Retrieved from http://www.ncbi.nlm.nih.gov/entrez/query.fcgi?cmd=Retrieve&db=PubMed&dopt=Citation&list_uids=23872024. doi:S0891-5849(13)00342-0 [pii] 10.1016/j.freeradbiomed.2013.07.011 [PubMed: 23872024]

Simone S, Gorin Y, Velagapudi C, Abboud HE, & Habib SL (2008). Mechanism of oxidative DNA damage in diabetes: tuberin inactivation and downregulation of DNA repair enzyme 8-oxo-7,8-dihydro-2'-deoxyguanosine-DNA glycosylase. Diabetes, 57(10), 2626–2636. Retrieved from https://www.ncbi.nlm.nih.gov/pubmed/18599524. doi:10.2337/db07-1579 [PubMed: 18599524]

Thameem F, Puppala S, Lehman DM, Stern MP, Blangero J, Abboud HE, . . . Habib SL (2010). The Ser(326)Cys polymorphism of 8-oxoguanine glycosylase 1 (OGG1) is associated with type 2 diabetes in Mexican Americans. Hum Hered, 70(2), 97–101. Retrieved from https://www.ncbi.nlm.nih.gov/pubmed/20606456. doi:10.1159/000291964 [PubMed: 20606456]

Valavanidis A, Vlachogianni T, & Fiotakis C. (2009). 8-hydroxy-2' -deoxyguanosine (8-OHdG): A critical biomarker of oxidative stress and carcinogenesis. J Environ Sci Health C Environ Carcinog Ecotoxicol Rev, 27(2), 120–139. Retrieved from https://www.ncbi.nlm.nih.gov/pubmed/19412858. doi:10.1080/10590500902885684 [PubMed: 19412858]

van der Kemp PA, Charbonnier JB, Audebert M, & Boiteux S. (2004). Catalytic and DNA-binding properties of the human Ogg1 DNA N-glycosylase/AP lyase: biochemical exploration of H270, Q315 and F319, three amino acids of the 8-oxoguanine-binding pocket. Nucleic Acids Res, 32(2), 570–578. Retrieved from https://www.ncbi.nlm.nih.gov/pubmed/14752045. doi:10.1093/nar/gkh224 [PubMed: 14752045]

Wallace SS (2014). Base excision repair: a critical player in many games. DNA Repair (Amst), 19, 14–26. Retrieved from https://www.ncbi.nlm.nih.gov/pubmed/24780558. doi:10.1016/j.dnarep.2014.03.030 [PubMed: 24780558]

Wang J, Wang Q, Watson LJ, Jones SP, & Epstein PN (2011). Cardiac overexpression of 8-oxoguanine DNA glycosylase 1 protects mitochondrial DNA and reduces cardiac fibrosis following transaortic constriction. Am J Physiol Heart Circ Physiol, 301(5), H2073–2080. Retrieved from https://www.ncbi.nlm.nih.gov/pubmed/21873502. doi:10.1152/ajpheart.00157.2011 [PubMed: 21873502]

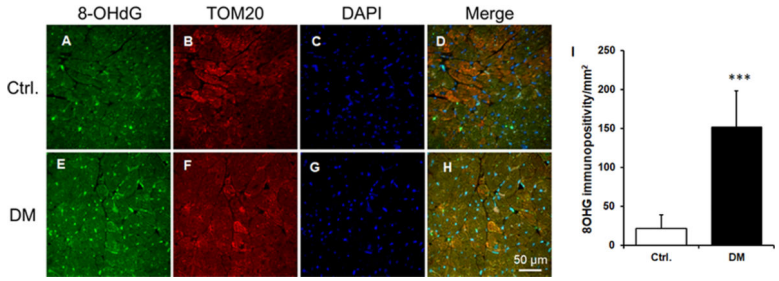

Figure 1. Increased mitochondrial 8OHG in diabetic cardiac tissue.

A-H. The representative micrographs of cardiac sections from *db/dm* control (Ctrl) and *db/db* diabetic (DM) mice with immunostaining of 8OHG (green), TOM20 (red), and nucleus (DAPI) were shown. At least 3 hearts per group and 15 high power fields per sample were employed for the analysis. **I.** The quantification data of 8OHG. Data were Mean ± SEM . ***P<0.001 vs Ctrl.

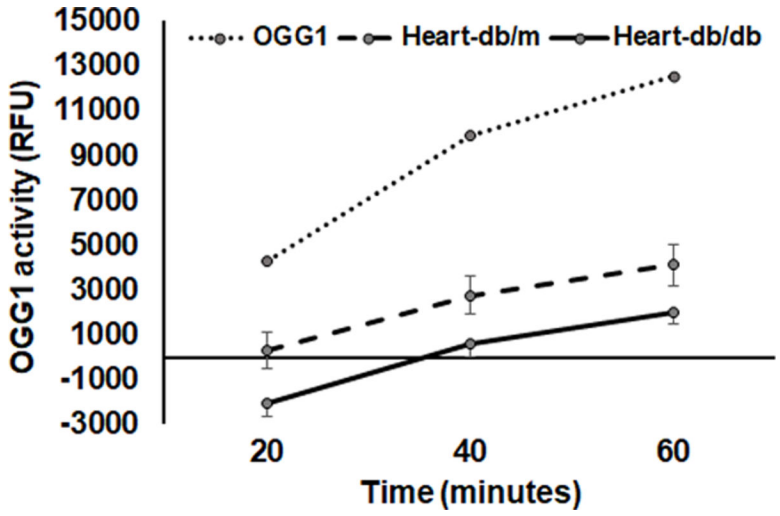

Figure 2. Decreased OGG-1 activity in diabetic heart tissue.

The dotted line, broken line and solid line were representing recombinant OGG-1, control heart tissue (*db/dm*) and diabetic heart tissue (*db/db*), respectively. Data were Mean ± SEM. N=4 *P<0.05 vs *db/db*.

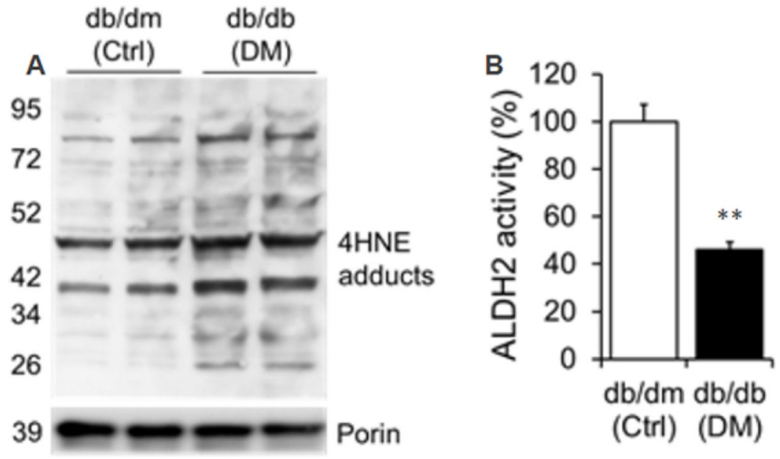

Figure 3. Increased 4HNE adducts and decreased ALDH2 activity in diabetic cardiac tissue.

A. Western blot band images of 4HNE adducts in cardiac tissue homogenates with *db/dm* control (Ctrl) and *db/db* diabetic (DM) mice for 4HNE adducts and Porin. **B.** Quantification data of cardiac ALDH2 activity from *db/dm* control (Ctrl) and *db/db* diabetic (DM) mice. Data were mean ± SEM. N=4 **P<0.01 vs Ctrl.

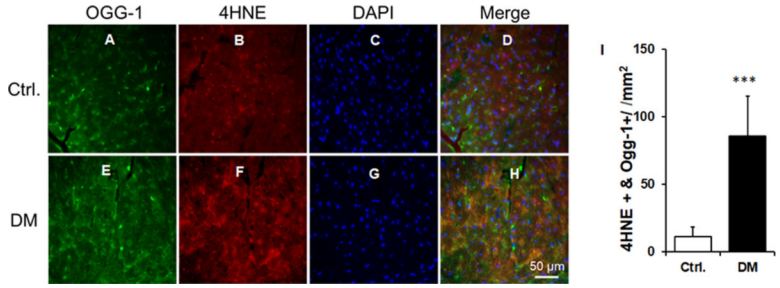

Figure 4. Increased 4HNE adduction on OGG-1 in diabetic cardiac tissue

A-H. The representative micrographs of cardiac sections from *db/dm* control (Ctrl) and *db/db* diabetic (DM) mice with immunostaining of OGG-1 (green), 4HNE (red), and nucleus (DAPI) were shown. **I.** The quantification data of 4HNE and OGG-1 double immunopositivity. Data were Mean ± SEM. At least 3 hearts per group and 15 high power fields per sample were employed for the analysis.***P<0.001 vs Ctrl.

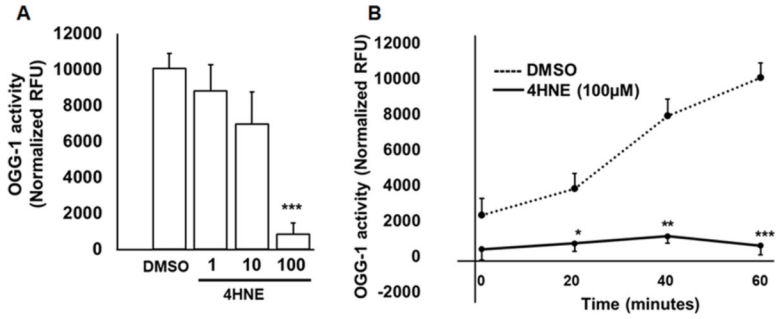

Figure 5. 4HNE attenuates OGG-1 activity.

A. OGG-1 activity is shown with increasing doses of 4HNE by incubating the 4HNE with recombinant OGG-1 at 60 minutes. Data were mean ± SEM. N=3 ***P<0.0006 vs DMSO.

B. Time course of 100μM 4HNE on OGG-1 activity with 20, 40 and 60 minutes. The dotted and solid lines represent DMSO and 4HNE (100 μM), respectively. Data were mean ± SEM. N=3 *P<0.02, **P<0.005 and ***P<0.0007 vs DMSO.

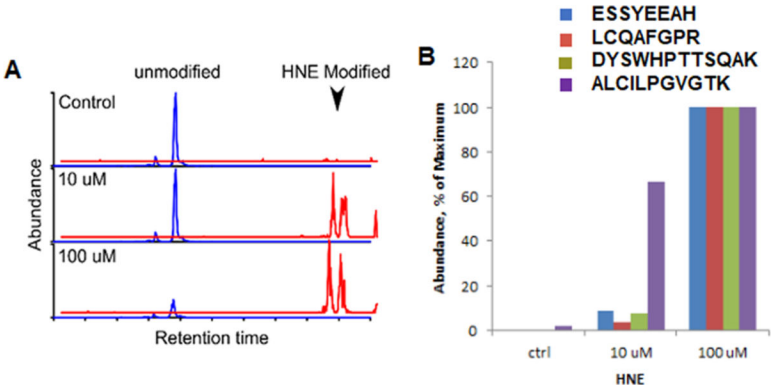

Figure 6. Dose-dependent increase in 4HNE modification on recombinant OGG-1.

A. The chromatograph depicts dose-dependent 4HNE modification on one of the OGG-1 peptides. **B.** The abundance of 4HNE modification on 4 OGG-1 peptides. 100μM data was kept as the maximum values. N=3.

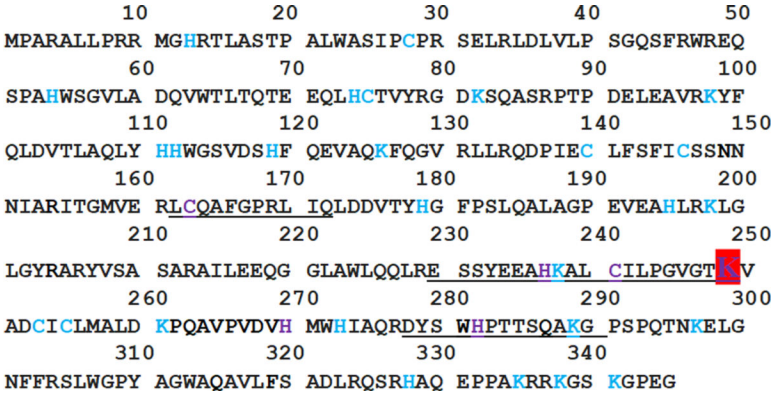

Figure 7. OGG-1 peptide sequence with 4HNE modification.

H, K and C are 4HNE modifiable amino acids. We color coded them in blue color fonts. The purple ones are 4HNE modified with 1-hour 4HNE incubation which we identified using mass spectroscopy. K249 is an active site in the red color background.

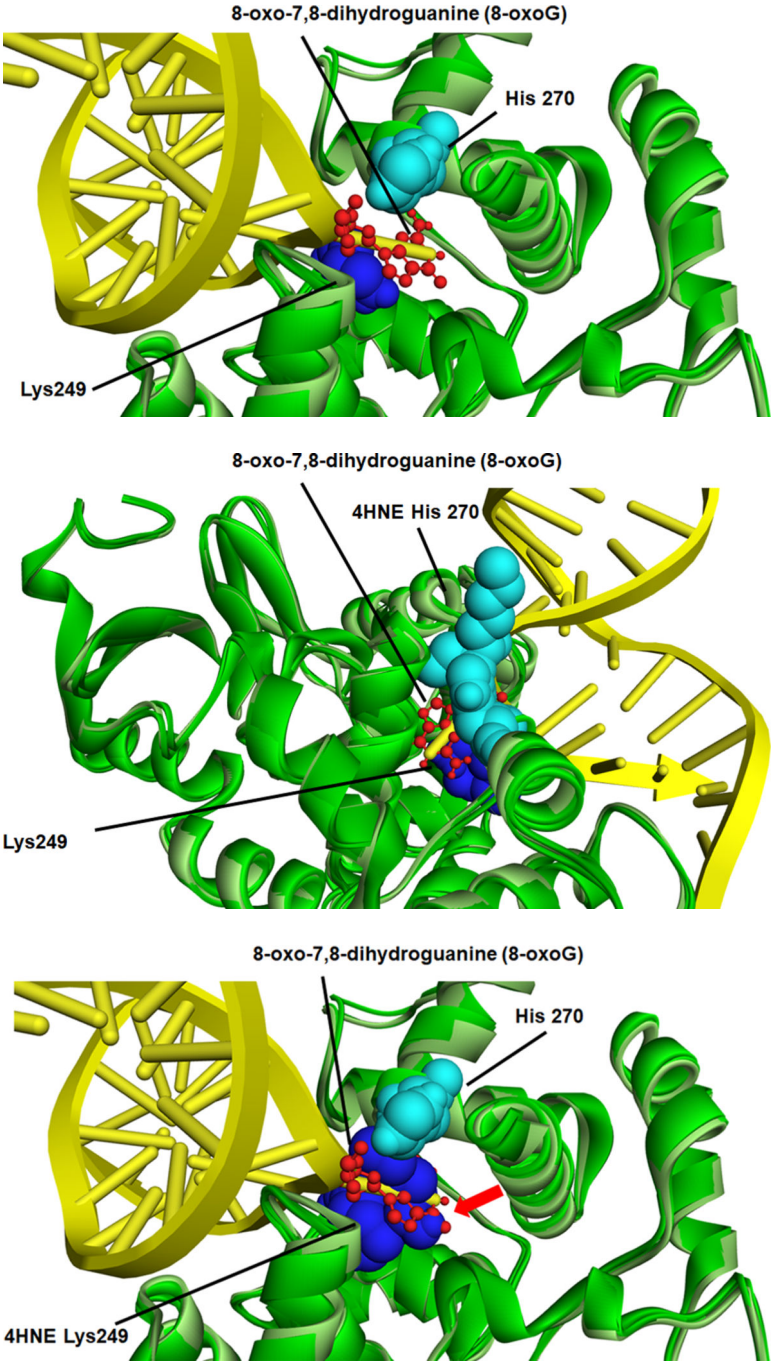

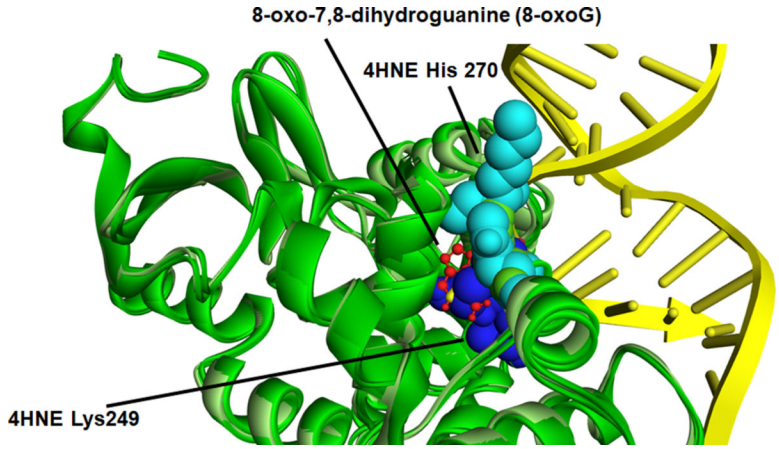

Figure 8. ***In silico*** **molecular modeling of 4-HNE-modified K^{249} and H^{270} on recombinant OGG-1.**

A. Overlay of unadducted OGG-1. H^{270} light blue (CPK), K^{249} dark blue (CPK), 8-oxoG red stick, OGG-1 backbone ribbon light green-dark green, DNA backbone yellow. **B.** Overlay of singly adducted OGG-1, 4HNE H^{270} light blue (CPK), K^{249} dark blue (CPK), 8-oxoG red stick, OGG-1 backbone ribbon light green-dark green, DNA backbone yellow. **C.** Overlay of K^{249} adducted OGG-1, H^{270} light blue (CPK), 4HNE K^{249} dark blue (CPK), 8-oxoG red stick, OGG-1 backbone ribbon light green-dark green, DNA backbone yellow. **D.** Overlay of doubly adducted OGG-1, 4HNE H^{270} light blue (CPK), 4HNE K^{249} dark blue (CPK), 8-oxoG red stick, OGG-1 backbone ribbon light green-dark green, DNA backbone yellow.